Leveraging Cation Exchange in InP Magic Sized Clusters to Access Coinage Metal Phosphide Nanocrystals

Forrest W. Eagle,[a] Samantha Harvey,[a] Helen Larson,[a] Autumn Abbott,[a] Dylan Ladd,[b] Kelsey Levine,[b] Michael Toney,[b,c] Daniel R. Gamelin,[a] and Brandi M. Cossairt[a]*

[a]Department of Chemistry, University of Washington, Box 351700, Seattle, WA 98195-1700, United States

[b]Department of Materials Science and Engineering, University of Colorado, Boulder, Colorado 80309, United States

[c]Department of Chemical and Biological Engineering, Renewable and Sustainable Energy Institute, University of Colorado, Boulder, Colorado 80309, United States

*cossairt@uw.edu

Abstract

We report the conversion of $In_{37}P_{20}$ magic sized clusters (MSCs) via cation exchange at room temperature to obtain doped InP clusters and nanocrystals, as well as $Cu_{3-x}P$, $Ag_{3-x}P$, and $Au_{3-x}P$ nanocrystals. Using a combination of spectroscopic and structural characterization, we determine that the InP clusters undergo doping with significant rearrangement of their ligand shells but only minor changes in their cores when 1 to 5 equivalents of coinage metal salt (per cluster) are added. However, when 37 equivalents of coinage metal salt are added, the MSCs fully transform both compositionally and structurally into new ultrasmall coinage metal phosphide nanocrystals with complete extrusion of indium, as determined via XPS, XRD, and PDF analysis. We further document the use of these doped InP MSCs and ultrasmall coinage metal phosphide nanocrystals for the synthesis of larger doped InP nanocrystals and a variety of coinage metal phosphide nanocrystals in the 3-30 nm size range.

Introduction

Magic sized clusters (MSCs) are atomically precise nanomaterials often found as metastable intermediates in the synthesis of nanocrystals.[1–3] Due to the atomically precise nature of these clusters, their physical, electronic, and reactivity properties can be studied without complications associated with ensemble heterogeneity. In particular, MSCs serve as a unique platform for the study of cation exchange. By understanding the mechanism and structural changes involved in cation exchange, synthetic chemists are able to rationally design new pathways to access colloidal nanomaterials that may be difficult or impossible to form by traditional bottom up nucleation and growth.[4–8] Additionally, although cation exchange in III-V nanocrystals often requires high temperatures, cation exchange in magic sized clusters can often be performed at

room temperature.[9–11] While cation exchange has been widely studied in Zn and Cd-chalcogenide MSCs,[11–17] few reports examine cation exchange in indium phosphide MSCs.[10,18] In this paper we demonstrate the cation exchange of InP magic sized clusters with coinage metals (Cu, Ag, and Au). Coinage metals are of particular interest due to the unique properties that characterize Group 11 binary compounds like phosphides and chalcogenides, including localized surface plasmon resonances (LSPRs) and enhanced catalytic activities. Given the ion mobility associated with copper ions in inorganic lattices,[19] the Cu-P products are also of interest for sequential cation exchange chemistries to access multinary and high entropy materials.

Copper phosphide has been widely studied, with special interest in the NIR LSPR generated in defective $Cu_{3-x}P$ lattices.[7,20–22] Additionally, Cu_3P is notable for its efficient electrocatalysis of both the hydrogen and oxygen evolution reactions, showing near unity Faradaic efficiency during hydrogen evolution and only minor degradation after extended use.[23–26] The other coinage metal phosphides, Ag-P and Au-P, have traditionally been difficult to synthesize due to their metastability.[27,28] Although Ag-P compounds have been predicted to serve as excellent catalysts for CO_2 reduction, accessing these materials has been synthetically challenging.[29,30] Homologous Ag-As and Ag-Sb systems have been found in nature, suggesting formation of Ag-pnictogen species is possible, however.[31–33] Au_2P_3 nanostructures have been synthesized;[27,34] however, these syntheses require phosphorization of Au nanocrystals and often lead to large domains of unreacted Au. Additionally, although AuP has been predicted,[28] there has been no synthesis of this material at the nanoscale nor the bulk. A more complete understanding of the electronic and catalytic properties of Au-P compounds will require the synthesis of crystalline, single domain nanocrystals across the range of possible stoichiometries.

In this work we demonstrate room temperature cation exchange in InP magic sized clusters, leading to the formation of doped InP clusters or small nanocrystals of $Cu_{3-x}P$, $Ag_{3-x}P$, and $Au_{3-x}P$. We further show that these small nanocrystals can then grow upon heating, leading to larger nanocrystals across the coinage metal phosphide family (**Scheme 1**). This MSC chemistry thus provides a versatile approach to the preparation, isolation, and study of coinage metal phosphide nanostructures.

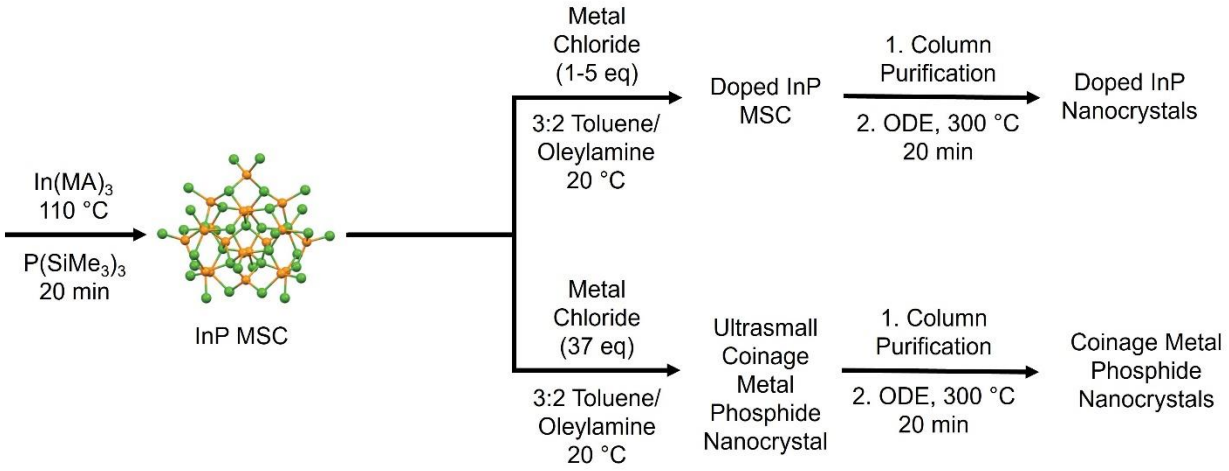

Scheme 1. Summary of cation exchange reactions of InP MSCs with coinage metals forming either doped InP MSCs or ultrasmall coinage metal phosphide nanocrystals. After isolation, these products can be heated to form doped InP or coinage metal phosphide nanocrystals.

Results and Discussion

Given the ultra-small size of MSCs, their optical properties are highly sensitive to changes in lattice structure because even small perturbations can greatly impact their electronic structure. As such, UV-Vis absorption spectroscopy can be used as a sensitive diagnostic tool to monitor changes in the cluster core. Upon adding low molar equivalents (1, 5 eq) of $CuCl_2$ solubilized in a 6:4 mixture of toluene and oleylamine to the starting $In_{37}P_{20}(O_2CC_{13}H_{27})_{51}$ cluster, we see the growth of a low-energy tail extending into the sub-bandgap region, followed by a broadening of the InP absorption band (**Figure 1A**). This broadening is consistent with the absorption of other Cu-doped and Cu-based nanocrystals, including Cu-CdSe and $CuInS_2$, and is not attributed to size inhomogeneity but rather a metal to ligand (conduction band) charge transfer type transition involving copper-localized holes.[35–37] As such, we attribute this continuous broadening of the absorption spectrum to the introduction of copper into the core of the MSC as opposed to exchange with the excess surface indium carboxylate Z-type ligands.[38] Upon addition of 37 equivalents of Cu (equal to the number of indium ions of the original MSC), we see complete loss of the original absorption peak, with conversion to a broad, featureless absorption spectrum spanning the visible region. This spectrum mirrors the UV-Vis absorption of previously characterized $Cu_{3-x}P$ nanocrystals, as well as Cu_2S and Cu_2Se nanocrystals.[20,21,39,40] Furthermore, the 37Cu-MSC exhibits the growth of a new feature in the near-infrared region of its absorption spectrum upon oxidation, as seen in the inset of **Figure 1A**. Previous reports of Cu_2Se nanoclusters have also detailed the growth of a similar feature upon oxidation, attributed to a new plasmon resonance.[41] This new feature is centered at ~800 nm, which is higher energy than the LSPRs of $Cu_{3-x}P$ nanocrystals, and this energy could reflect a blueshift due to quantum confinement.[21,41–43]

Addition of AgCl and AuCl to the $In_{37}P_{20}$ MSCs gives similar results - low equivalents of Ag and Au lead to the same spectral broadening, followed by conversion to a broad featureless absorption spectrum upon the addition of 37 equivalents (**Figure 1B, C**). While no reports of nanoparticle Ag-P complexes exist, this broad absorption is similar to that found in Ag_2Se and Ag_2S nanocrystals.[44–47]

We also observed similar results for $In_{37}P_{20}$ MSCs treated with CuCl and $AuCl_3$ solubilized in toluene/oleylamine mixtures, as shown in **Figure S1**, indicating that the starting metal halide solution is likely reduced in situ by the oleylamine and that all products contain coinage metals in the +1 oxidation state. This conclusion is confirmed by comparative XPS analysis (**Figure S2**).[48] Interestingly, upon attempting full cation exchange with coinage metal halides solubilized by tributyl phosphine, only minimal broadening in the absorbance profile is observed, suggesting hindered cation exchange when high equivalents of coinage metal are added under these conditions (**Figure S3**). This result suggests that the precursor identity is important, and that

amines help to drive the cation exchange. Previous work has shown that the addition of metal carboxylates to InP magic sized clusters can induce cation exchange, but requires much more added cation.[10]

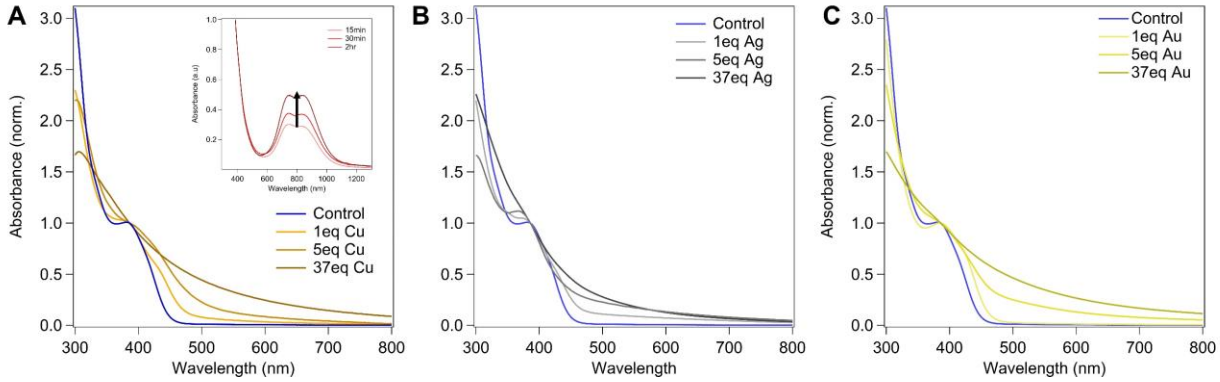

Figure 1. Absorption spectra of coinage metal treated $In_{37}P_{20}$ MSCs. A) Addition of 1, 5, and 37 equivalents of $CuCl_2$. Inset: absorption spectra of clusters treated with 37 equivalents of Cu followed by exposure to oxygen for the times indicated. Note that the dip at the absorption maximum is an instrumental artifact. B) Addition of 1, 5, and 37 equivalents of AgCl. C) Addition of 1, 5, and 37 equivalents of $AuCl_3$.

The initial pXRD pattern of $In_{37}P_{20}$ MSCs does not correspond to the zincblende phase of bulk InP. Instead the cluster has a strained core that can be described as having quasi-wurtzite character.[38] Upon the addition of 1 and 5 equivalents of $CuCl_2$ to the MSC, we see shifting and broadening of the diffraction peaks, indicating the original lattice becomes more disordered as more Cu ions are introduced into the core (**Table S1**). Upon addition of 37 equivalents, the original diffraction peaks are no longer visible and instead are replaced by two main peaks at $2\theta = 40°$ and 47° as seen in **Figure 2A**. These peaks are consistent with ultrasmall hexagonal Cu_3P nanocrystals.[49]

With the addition of 1 and 5 equivalents of AgCl, we once again see the shifting and broadening of the original $In_{37}P_{20}$ MSC peaks characteristic of the formation of a defective lattice. Upon addition of 37 equivalents of AgCl we see more drastic changes in the diffraction pattern, as shown in **Figure 2B**. While Cu-P compounds have routinely been synthesized and characterized, Ag-P compounds have not been successfully realized on the nanoscale despite much synthetic effort, leading to little to no literature from which to draw comparisons.[29,30]

Examination of the Au doped species shows much less broadening at 5 equivalents when compared to the Ag and Cu doped species – instead the growth of a new peak centered around 40° is observed (**Figure 2C**) – this peak corresponds with the major diffraction peak in hexagonal Au_3P.[50] As higher equivalents of Au are added, this new peak becomes better defined, while the peaks attributed to InP are lost. This result may suggest a highly cooperative cation exchange pathway for Au – as soon as doping reaches a critical concentration, full cation exchange is pushed to completion similar to Cu exchange in CdSe and Ag exchange in CdS.[51,52]

Our findings are also consistent with previous experiments showing that Ag leads to a cooperative cation exchange avalanche at lower concentrations than Cu.[52] As the size of the Au ion is larger, the InP lattice cannot as easily rearrange around the dopant, leading to structural transformation at lower dopant concentrations. These observations support theoretical predictions that the InP MSC lattice cannot rearrange favorably around larger dopants.[52,53]

The broad XRD peaks of **Figure 2A-C** are consistent with ultrasmall nanocrystals, a conclusion corroborated by TEM analysis showing that the average size of the fully cation exchanged clusters is 3 nm for the Cu_3P nanocrystals and 2 nm for the Ag_3P and Au_3P nanocrystals **(Figure S4-6).** The structures of these products were further investigated by PDF analysis of the 37 equivalent treated samples (**Figure 2D**). Previous work in our group has shown the sensitivity of PDF to changes to the internal lattice of InP MSCs.[2,10] Most noticeably, all three exchanged samples show the loss of the prominent peak around 4.1 Å, representative of the In-In network in the original InP lattice. These data show that the internal lattice of the Cu-P cluster is similar to that of Cu_3P nanocrystals, having major reflections at 2.25 and 2.61 Å corresponding to Cu-P and Cu-Cu distances, respectively.[54] Although previous PDF analysis does not exist for Ag-P or Au-P complexes, the Ag-P and Au-P clusters show new peaks around 2.9-3.0 Å that agree well with theoretical predictions for AgP and Au-P bonds in Ag_3P and Au_3P (**Figure S7**). We note that all three clusters also show peaks at 2.2 and 2.6 Å, and it is difficult to determine if these peaks correspond to the In-O and In-P bonds of surface bound In-carboxylate moieties or if they reflect distorted metal-metal and metal-phosphorus distances similar to those found in Cu-P. Overall, the combination of XRD, PDF, and TEM data point to the formation of unique Cu-P, Ag-P, and Au-P clusters through these cation exchange reactions.

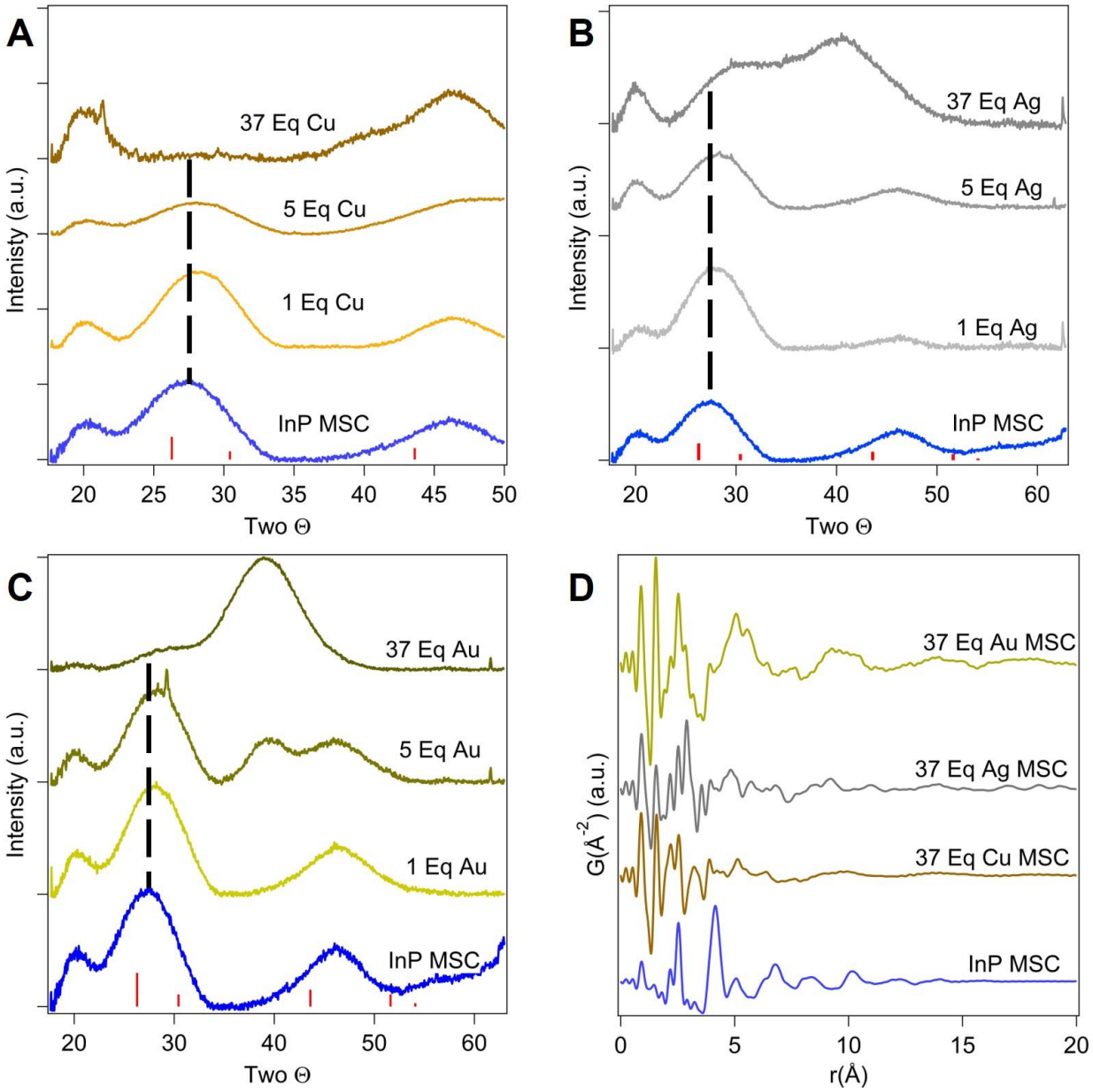

Figure 2. A) pXRD pattern upon addition of $CuCl_2$ to $In_{37}P_{20}$. Zinc blende InP is shown in red. B) pXRD pattern upon addition of AgCl to $In_{37}P_{20}$. Zinc blende InP is shown in red. C) pXRD pattern upon addition of $AuCl_3$ to $In_{37}P_{20}$. Zinc blende InP is shown in red. D) PDF analysis of InP MSCs and clusters treated with 37 equivalents of coinage metal.

To further resolve the composition and coordination environments of the coinage metal treated clusters, XPS data were collected. After addition of $CuCl_2$ to the $In_{37}P_{20}$ MSCs, we see the growth of the expected copper 2p peaks with further increased resolution upon additional equivalents as seen in **Figure 3A**. With increasing equivalents of added Cu, we also see a shift to lower binding energies by over 1 eV, with the $2p_{3/2}$ peak reaching 932.6 eV for the 37-equivalent

sample. This value is consistent with that measured for Cu_3P.[19] The addition of AgCl to $In_{37}P_{20}$ MSCs leads to the growth of Ag 3d peaks as seen in **Figure 3B**. As nanoscale Ag-P has not been successfully synthesized previously, there is no comparative XPS to examine. However, we do see the growth of silver 3d peaks as more silver is added, indicating increasing incorporation of silver into the material. Furthermore, these peaks closely correspond to the binding energy found for Ag_2S.[55] Similarly, addition of $AuCl_3$ to the $In_{37}P_{20}$ MSC also shows an increasing Au signal with more equivalents added, as shown in **Figure 3C**. In the Au sample, the initial binding energy of the $4f_{7/2}$ peak is 84.2 eV, which is reminiscent of Au-amine complexes.[56] As more equivalents are added, the binding energy shifts to 84.5 eV which corresponds to Au in InP,[57] before shifting to higher binding energies, suggesting greater electronic interaction between the Au and P atoms in the lattice. For reference, XPS of as-synthesized $In_{37}P_{20}$ MSCs shows In peaks characteristic of InP, centered at 444.7 eV, as shown in **Figure 3D**.[58] After the introduction of any of these coinage metal dopants, the peaks begin to shift to higher binding energy, with shifts of over 1 eV, to 445.9 eV, highly reminiscent of $InCl_3$ or $In(O_2CR)_3$.[10,59] As such, we posit that the many of the In ions have been exchanged out of the cluster core and remain instead as loosely associated molecular or surface bound species. Upon adding 37 equivalents of Cu, we see complete loss of the In signal, suggesting complete cation exchange. These data correspond well with other forms of atomic elemental analysis, with ICP data showing small to no evidence of indium left in the core of the fully exchanged nanocrystals **(Table S2**).

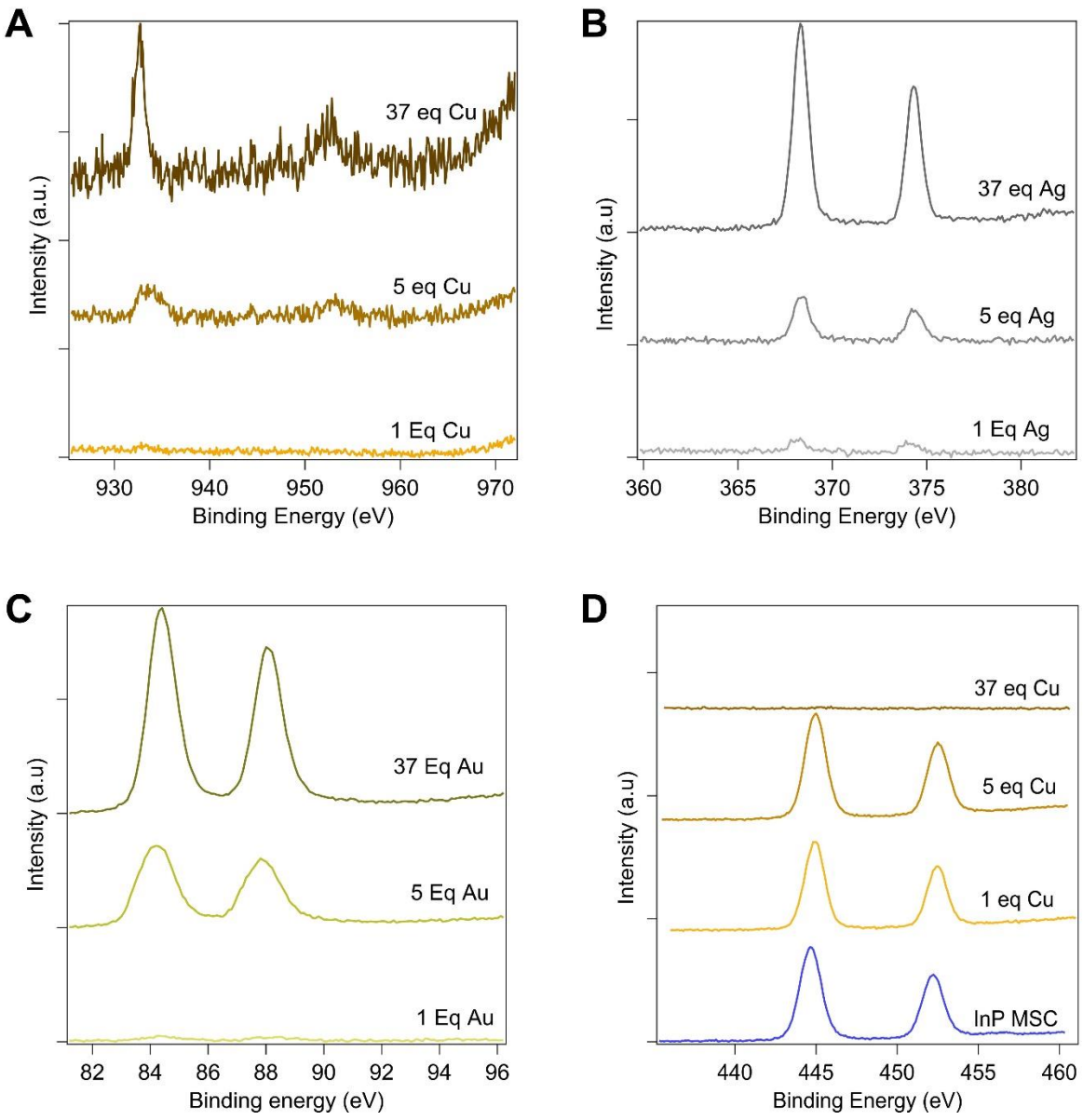

Figure 3. A) XPS spectra of Cu 2p peaks with addition of $CuCl_2$ to $In_{37}P_{20}$ MSCs. B) Ag 3d peaks upon addition of AgCl to $In_{37}P_{20}$ MSCs. C) Au 4f peaks with addition of $AuCl_3$ to $In_{37}P_{20}$ MSCs. D) XPS spectra of In 3d peaks upon addition of $CuCl_2$ to $In_{37}P_{20}$ MSCs.

As previous reports have shown that the introduction of coinage metals to InP quantum dots drastically effects their charge carrier lifetimes,[36,60,61] we turned to transient absorption spectroscopy to examine if a similar phenomenon would occur with these even smaller materials. The transient absorption spectra of cation exchanged MSCs were strongly affected by increasing molar equivalents of coinage metal cations. In lightly doped samples, a broadening that matches the change in the absorption profile is observed (**Figure S8**). Clusters doped with a single equivalent of coinage metal show a drastic reduction in both the bleach and photoinduced

absorption lifetimes, as shown in **Figure 4A-C,** with lifetimes for Cu, Ag, and Au doped clusters as 210, 150, and 120 ps, respectively. In contrast, the undoped clusters have lifetimes of 1550 ps, as seen in **Figure 4D**. This relatively long lifetime is attributable to localization of the charge carriers in the highly strained excited state of the InP MSC, analogous to molecular species.[62,63] The drastic differences in excited state lifetimes could conceivably be attributed to the evolution of MSCs from a molecular like species with highly localized frontier orbitals to one with a much more delocalized electronic structure as structural rearrangement occurs near the surface to alleviate strain.[62] Additional transient absorption studies show that the lifetime of the same cluster treated with amine is reduced, but longer than the doped species, as shown in the kinetic data of **Figure 4D**. The large number of new mid-gap states introduced upon doping, evident from the broadened absorption spectra of **Figure 1**, are expected to facilitate rapid non-radiative recombination, thus leading to shorter lifetimes. Interestingly, our pXRD data (**Figure 2**) suggest that the structure of the InP MSCs is maintained at low equivalents of dopant. Instead, we posit that the addition of our dopant solution causes loss of indium carboxylate with concerted coordination of the dopant metal halide complex, followed by rearrangement of this new mixed carboxylate-halide ligand shell as the dopant migrates to the core, leading to a cluster with less highly localized frontier orbitals. This analysis is consistent with previous reports by our group detailing the liberation of indium carboxylates upon addition of amine ligands in a formal L-assisted Z-type ligand displacement reaction.[64,65] This mechanism is further supported by previous theoretical studies showing that the initial reactivity of InP increases with decreasing size and In-In separation, and that doping of aliovalent ions is more favorable following ligand removal.[53,66,67]

Upon addition of 37 equivalents of coinage metal precursor, the original bleach and photoinduced absorption profile is eliminated. Instead, the TA signal is replaced by a rapid, broad photoinduced absorption feature as seen in **Figures S9-10**, indicating that the new clusters have an excited state absorption coefficient greater than the ground state absorption coefficient at these wavelengths, similar to coinage metal chalcogenides.[68–70]

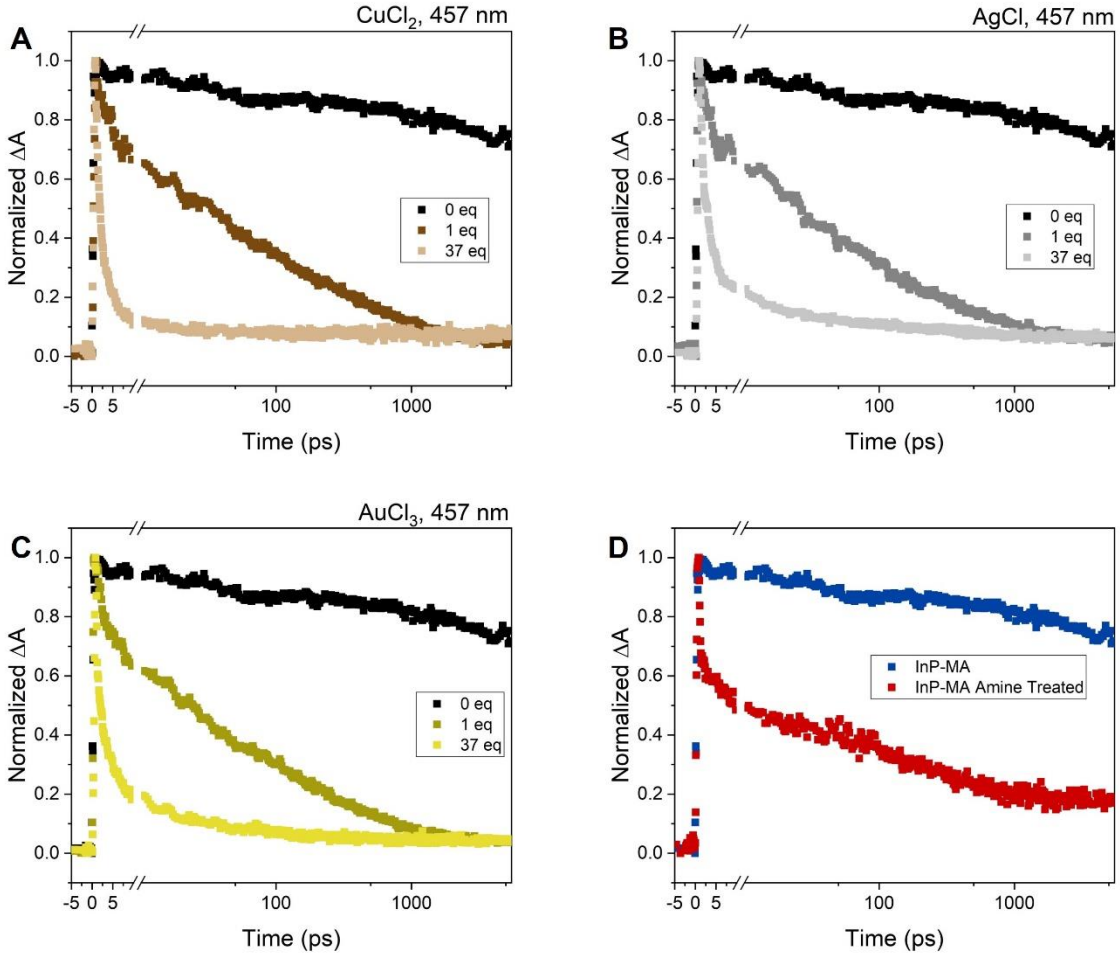

Figure 4. Transient absorption decay dynamics of InP MSCs following addition of 1 and 37 equivalents of $CuCl_2$ (A), AgCl (B), and $AuCl_3$ (C). D) Transient absorption kinetics of myristate capped $In_{37}P_{20}$ and amine treated cluster.

Further interest in these coinage metal-containing clusters derives from their utility as single source precursors for the formation of larger nanocrystals.[2,71–73] After conversion of the $In_{37}P_{20}$ MSCs to coinage metal phosphide clusters, we next examined if these materials could be used for the formation of larger nanocrystals. We hypothesized that a hot-injection synthesis can be used to overcome the energic barrier keeping MSCs in their metastable state and allow them to convert to larger, more stable nanocrystals. Indeed, upon injecting MSCs treated with 1 equivalent of copper into ODE heated to 300 °C, we obtain Cu^+:InP quantum dots. This can be observed in **Figure S10** by the broadened absorption profile along with broad, NIR luminescence, mirroring previously reported Cu^+:InP systems.[35,36,60] Furthermore, these samples show highly similar diffraction patterns to undoped InP, suggesting that the zincblende InP lattice is retained (**Figure S11**).

However, using the fully cation exchanged clusters yields different products. Upon conversion of the MSCs that were treated with 37 equivalents of copper, the major product is Cu_3P nanocrystals, confirmed via pXRD analysis as shown in **Figure 5A**. TEM analysis (**Figure 5D**) shows formation of larger (12.5 ± 0.5 nm) oblong nanocrystals. Hot injection of the MSCs treated with 37 equivalents of silver leads to greater structural transformations of the cluster, with the pXRD in **Figure 5B** showing the formation of Ag_3P in the tetragonal phase. Excitingly, this is the first report of this material on the nanoscale to the best of our knowledge.[74] TEM analysis of these new Ag_3P nanocrystals shows an average size of 3.8 ± 0.2 nm (**Figure 5E**) suggesting much less growth relative to the Cu-P system. Performing a hot-injection reaction of the MSCs treated with 37 equivalents of Au with identical reaction parameters does not form nanocrystals of a new morphology but instead grows the cluster-based structure, as seen by the peak sharpening in the pXRD (**Figure 5C**) and growth to 3.8 ± 0.3 nm in size as seen via TEM (**Figure 5F**).

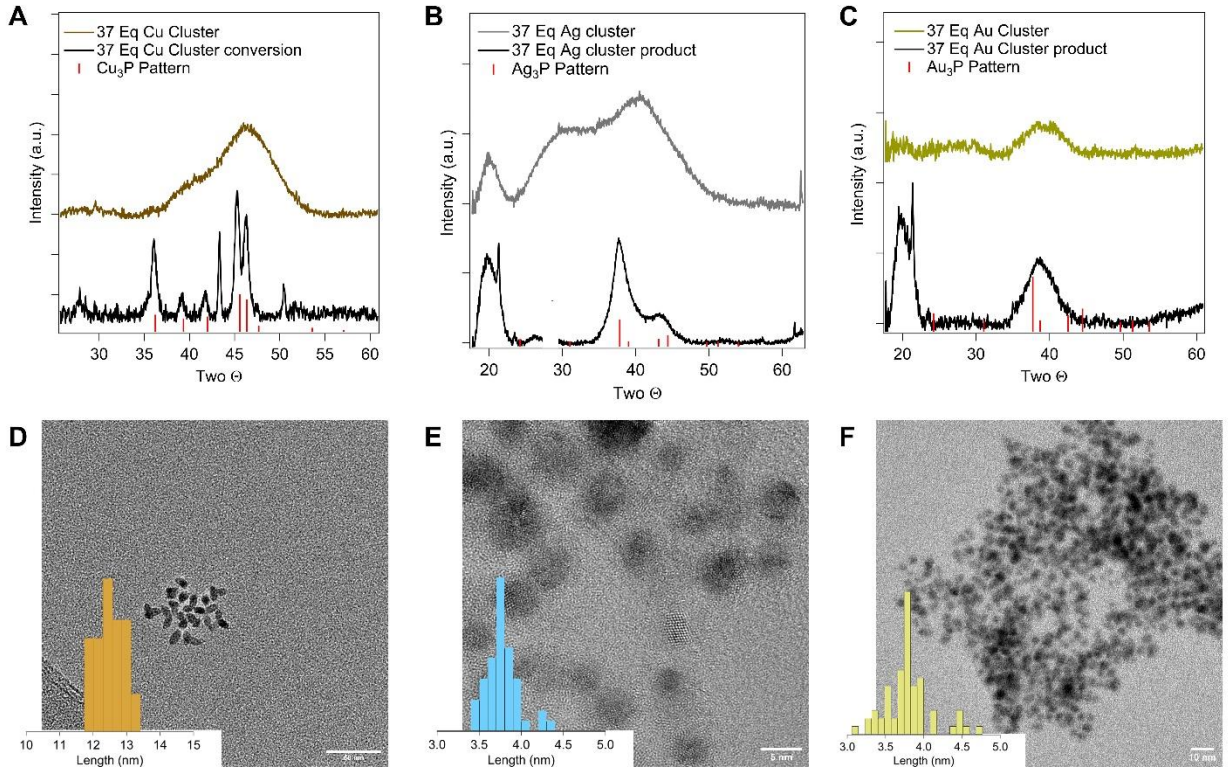

Figure 5. A) pXRD of Cu_3P nanocrystals resulting from the hot injection of MSCs treated with 37 equivalents of Cu. The peak at 43 corresponds to the formation of a small fraction of large Cu nanocrystals. B) pXRD of MSCs treated with 37 equivalents of Ag before and after hot injection reaction (the Si 111 peak at 28.4 has been removed from the analysis for clarity). C) pXRD of MSCs treated with 37 equivalents of Au before and after hot injection reaction. D) TEM of MSCs treated with 37 equivalents of Cu after hot injection reaction (scale bar is 50 nm) E) TEM of MSCs treated with 37 equivalents of Ag after hot injection reaction (scale bar is 5 nm). F) TEM of MSCs treated with 37 equivalents of Au after hot injection reaction (scale bar is 10 nm).

Conclusion

We have demonstrated the room temperature conversion of $In_{37}P_{20}$ MSCs into doped InP clusters and $M_{3-x}P$ (M = Cu, Ag, Au) nanocrystals through exchange of indium using a coinage metal salt. From a combination of absorption spectroscopy and pXRD data we determined that the MSC core undergoes doping without significant structural changes upon addition of 1 to 5 equivalents of coinage metal. However, at 37 equivalents of added coinage metal, we observe the complete transformation into new metal phosphide clusters with no evidence for remaining indium in the core. Transient absorption spectroscopy of MSCs exposed to 1 equivalent of coinage metal reactant suggests that removal of some excess surface In is required before the transformation of the inorganic core can occur, while further exchange exhibits characteristics expected in coinage metal phosphides. Hot injection reactions of these new coinage metal phosphide clusters form larger metal phosphide nanocrystals that reflect the cluster compositions. Notably, colloidal nanocrystals of Ag_3P and Au_3P have not been previously reported. This work illustrates that cation exchange can be utilized not only as a method of studying structural transformations in magic sized clusters, but also as an approach to expanding the library of magic sized clusters that serve as intermediates in the formation of a variety of nanocrystals, including metastable or otherwise difficult to form species.

Acknowledgments

This research was supported by the U.S. National Science Foundation (NSF) through the UW Molecular Engineering Materials Center (MEM-C), a Materials Research Science and Engineering Center (Grant No. DMR-1719797 and DMR-2308979). The authors acknowledge the use of facilities and instrumentation supported by the U.S. National Science Foundation through the UW MEM-C (DMR-1719797 and DMR-2308979). Part of this work was conducted at the Molecular Analysis Facility, a National Nanotechnology Coordinated Infrastructure site at the University of Washington, which is supported, in part, by the National Science Foundation (Grant No. NNCI-1542101), the University of Washington, the Molecular Engineering and Sciences Institute, and the Clean Energy Institute. S.H. gratefully acknowledges fellowship support from the Department of Energy Office of Basic Sciences (Grant No. DE-SC0021232).

Supporting Information

Complete experimental methods and additional data including supporting UV-Vis, XPS, ICP-OES, TEM, and XRD can be found in the Supporting Information.

References

(1) Cunningham, P. D.; Coropceanu, I.; Mulloy, K.; Cho, W.; Talapin, D. V. Quantized Reaction Pathways for Solution Synthesis of Colloidal ZnSe Nanostructures: A Connection between Clusters, Nanowires, and Two-Dimensional Nanoplatelets. *ACS Nano* **2020**, *14* (4), 3847–3857. https://doi.org/10.1021/acsnano.9b09051.

(2) Gary, D. C.; Terban, M. W.; Billinge, S. J. L.; Cossairt, B. M. Two-Step Nucleation and Growth of InP Quantum Dots via Magic-Sized Cluster Intermediates. *Chem. Mater.* **2015**, *27* (4), 1432–1441. https://doi.org/10.1021/acs.chemmater.5b00286.

(3) Friedfeld, M. R.; Stein, J. L.; Cossairt, B. M. Main-Group-Semiconductor Cluster Molecules as Synthetic Intermediates to Nanostructures. *Inorganic Chemistry* **2017**, *56* (15), 8689–8697. https://doi.org/10.1021/acs.inorgchem.7b00291.

(4) Fenton, J. L.; Steimle, B. C.; Schaak, R. E. Tunable Intraparticle Frameworks for Creating Complex Heterostructured Nanoparticle Libraries. *Science* **2018**, *360* (6388), 513–517. https://doi.org/10.1126/science.aar5597.

(5) Steimle, B. C.; Fenton, J. L.; Schaak, R. E. Rational Construction of a Scalable Heterostructured Nanorod Megalibrary. *Science* **2020**, *367* (6476), 418–424. https://doi.org/10.1126/science.aaz1172.

(6) Stone, D.; Koley, S.; Remennik, S.; Asor, L.; Panfil, Y. E.; Naor, T.; Banin, U. Luminescent Anisotropic Wurtzite InP Nanocrystals. *Nano Lett.* **2021**, *21* (23), 10032–10039. https://doi.org/10.1021/acs.nanolett.1c03719.

(7) De Trizio, L.; Gaspari, R.; Bertoni, G.; Kriegel, I.; Moretti, L.; Scotognella, F.; Maserati, L.; Zhang, Y.; Messina, G. C.; Prato, M.; Marras, S.; Cavalli, A.; Manna, L. $Cu_{3-x}P$ Nanocrystals as a Material Platform for Near-Infrared Plasmonics and Cation Exchange Reactions. *Chemistry of Materials* **2015**, *27* (3), 1120–1128. https://doi.org/10.1021/cm5044792.

(8) Beberwyck, B. J.; Alivisatos, A. P. Ion Exchange Synthesis of III–V Nanocrystals. *J. Am. Chem. Soc.* **2012**, *134* (49), 19977–19980. https://doi.org/10.1021/ja309416c.

(9) White, S. L.; Banerjee, P.; Chakraborty, I.; Jain, P. K. Ion Exchange Transformation of Magic-Sized Clusters. *Chem. Mater.* **2016**, *28* (22), 8391–8398. https://doi.org/10.1021/acs.chemmater.6b03882.

(10) Stein, J. L.; Steimle, M. I.; Terban, M. W.; Petrone, A.; Billinge, S. J. L.; Li, X.; Cossairt, B. M. Cation Exchange Induced Transformation of InP Magic-Sized Clusters. *Chem. Mater.* **2017**, *29* (18), 7984–7992. https://doi.org/10.1021/acs.chemmater.7b03075.

(11) He, L.; Luan, C.; Liu, S.; Chen, M.; Rowell, N.; Wang, Z.; Li, Y.; Zhang, C.; Lu, J.; Zhang, M.; Liang, B.; Yu, K. Transformations of Magic-Size Clusters via Precursor Compound Cation Exchange at Room Temperature. *J. Am. Chem. Soc.* **2022**, *144* (41), 19060–19069. https://doi.org/10.1021/jacs.2c07972.

(12) Muckel, F.; Yang, J.; Lorenz, S.; Baek, W.; Chang, H.; Hyeon, T.; Bacher, G.; Fainblat, R. Digital Doping in Magic-Sized CdSe Clusters. *ACS Nano* **2016**, *10* (7), 7135–7141. https://doi.org/10.1021/acsnano.6b03348.

(13) Yang, J.; Fainblat, R.; Kwon, S. G.; Muckel, F.; Yu, J. H.; Terlinden, H.; Kim, B. H.; Iavarone, D.; Choi, M. K.; Kim, I. Y.; Park, I.; Hong, H.-K.; Lee, J.; Son, J. S.; Lee, Z.; Kang, K.; Hwang, S.-J.; Bacher, G.; Hyeon, T. Route to the Smallest Doped Semiconductor: Mn2+-Doped (CdSe)13 Clusters. *J. Am. Chem. Soc.* **2015**, *137* (40), 12776–12779. https://doi.org/10.1021/jacs.5b07888.

(14) Pittala, S.; Mortelliti, M. J.; Kato, F.; Kittilstved, K. R. Substitution of Co2+ Ions into CdS-Based Molecular Clusters. *Chem. Commun.* **2015**, *51* (96), 17096–17099. https://doi.org/10.1039/C5CC06138E.

(15) Eilers, J.; Groeneveld, E.; de Mello Donegá, C.; Meijerink, A. Optical Properties of Mn-Doped ZnTe Magic Size Nanocrystals. *J. Phys. Chem. Lett.* **2012**, *3* (12), 1663–1667. https://doi.org/10.1021/jz300300g.

(16) Fainblat, R.; Barrows, C. J.; Gamelin, D. R. Single Magnetic Impurities in Colloidal Quantum Dots and Magic-Size Clusters. *Chem. Mater.* **2017**, *29* (19), 8023–8036. https://doi.org/10.1021/acs.chemmater.7b03195.

(17) Lin, J.; Zhang, Q.; Wang, L.; Liu, X.; Yan, W.; Wu, T.; Bu, X.; Feng, P. Atomically Precise Doping of Monomanganese Ion into Coreless Supertetrahedral Chalcogenide Nanocluster Inducing Unusual Red Shift in Mn2+ Emission. *J. Am. Chem. Soc.* **2014**, *136* (12), 4769–4779. https://doi.org/10.1021/ja501288x.

(18) Friedfeld, M. R.; Stein, J. L.; Johnson, D. A.; Park, N.; Henry, N. A.; Enright, M. J.; Mocatta, D.; Cossairt, B. M. Effects of Zn2+ and Ga3+ Doping on the Quantum Yield of Cluster-Derived InP Quantum Dots. *J. Chem. Phys.* **2019**, *151* (19), 194702. https://doi.org/10.1063/1.5126971.

(19) Rivest, J. B.; Jain, P. K. Cation Exchange on the Nanoscale: An Emerging Technique for New Material Synthesis, Device Fabrication, and Chemical Sensing. *Chem. Soc. Rev.* **2012**, *42* (1), 89–96. https://doi.org/10.1039/C2CS35241A.

(20) Manna, G.; Bose, R.; Pradhan, N. Semiconducting and Plasmonic Copper Phosphide Platelets. *Angewandte Chemie International Edition* **2013**, *52* (26), 6762–6766. https://doi.org/10.1002/anie.201210277.

(21) Rachkov, A. G.; Schimpf, A. M. Colloidal Synthesis of Tunable Copper Phosphide Nanocrystals. *Chem. Mater.* **2021**, *33* (4), 1394–1406. https://doi.org/10.1021/acs.chemmater.0c04460.

(22) Bertoni, G.; Ramasse, Q.; Brescia, R.; De Trizio, L.; De Donato, F.; Manna, L. Direct Quantification of Cu Vacancies and Spatial Localization of Surface Plasmon Resonances in Copper Phosphide Nanocrystals. *ACS Materials Lett.* **2019**, *1* (6), 665–670. https://doi.org/10.1021/acsmaterialslett.9b00412.

(23) Tian, J.; Liu, Q.; Cheng, N.; Asiri, A. M.; Sun, X. Self-Supported Cu3P Nanowire Arrays as an Integrated High-Performance Three-Dimensional Cathode for Generating Hydrogen from Water. *Angewandte Chemie International Edition* **2014**, *53* (36), 9577–9581. https://doi.org/10.1002/anie.201403842.

(24) Zhou, X.; Zhou, X.; Liu, L.; Chen, H.; Hu, X.; Qian, J.; Huang, D.; Zhang, B.; Tang, J. Self-Supported Cu $_3$ P Nanowire Electrode as an Efficient Electrocatalyst for the Oxygen Evolution Reaction. *RSC Adv.* **2021**, *11* (54), 34137–34143. https://doi.org/10.1039/D1RA05526G.

(25) Laursen, A. B.; Calvinho, K. U. D.; Goetjen, T. A.; Yap, K. M. K.; Hwang, S.; Yang, H.; Garfunkel, E.; Dismukes, G. C. CO2 Electro-Reduction on Cu3P: Role of Cu(I) Oxidation State and Surface Facet Structure in C1-Formate Production and H2 Selectivity. *Electrochimica Acta* **2021**, *391*, 138889. https://doi.org/10.1016/j.electacta.2021.138889.

(26) Downes, C. A.; Libretto, N. J.; Harman-Ware, A. E.; Happs, R. M.; Ruddy, D. A.; Baddour, F. G.; Ferrell III, J. R.; Habas, S. E.; Schaidle, J. A. Electrocatalytic CO2 Reduction over Cu3P Nanoparticles Generated via a Molecular Precursor Route. *ACS Appl. Energy Mater.* **2020**, *3* (11), 10435–10446. https://doi.org/10.1021/acsaem.0c01360.

(27) Carenco, S.; Florea, I.; Ersen, O.; Boissière, C.; Mézailles, N.; Sanchez, C. Towards Nanoscaled Gold Phosphides: Surface Passivation and Growth of Composite Nanostructures. *New J. Chem.* **2013**, *37* (4), 1231–1237. https://doi.org/10.1039/C3NJ41037D.

(28) Okamoto, H.; Massalski, T. B. The Au−P (Gold-Phosphorus) System. *Bulletin of Alloy Phase Diagrams* **1984**, *5* (5), 490–491. https://doi.org/10.1007/BF02872903.

(29) Sweeney, C. M.; Stamm, K. L.; Brock, S. L. On the Feasibility of Phosphide Generation from Phosphate Reduction: The Case of Rh, Ir, and Ag. *Journal of Alloys and Compounds* **2008**, *448* (1), 122–127. https://doi.org/10.1016/j.jallcom.2006.10.035.

(30) Li, H.; Wen, P.; Itanze, D. S.; Hood, Z. D.; Ma, X.; Kim, M.; Adhikari, S.; Lu, C.; Dun, C.; Chi, M.; Qiu, Y.; Geyer, S. M. RETRACTED ARTICLE: Colloidal Silver Diphosphide (AgP2) Nanocrystals as Low Overpotential Catalysts for CO2 Reduction to Tunable Syngas. *Nat Commun* **2019**, *10* (1), 5724. https://doi.org/10.1038/s41467-019-13388-8.

(31) Vaughey, J. T.; Fransson, L.; Swinger, H. A.; Edström, K.; Thackeray, M. M. Alternative Anode Materials for Lithium-Ion Batteries: A Study of Ag3Sb. *Journal of Power Sources* **2003**, *119–121*, 64–68. https://doi.org/10.1016/S0378-7753(03)00126-5.

(32) Ag (Silver) Binary Alloy Phase Diagrams. **2016**. https://doi.org/10.31399/asm.hb.v03.a0006143.

(33) Cipriani, C.; Corazza, M.; Mazzetti, G. Reinvestigation of Natural Silver Antimonides. *ejm* **1997**, *8* (6), 1347–1350. https://doi.org/10.1127/ejm/8/6/1347.

(34) Henkes, A. E.; Vasquez, Y.; Schaak, R. E. Converting Metals into Phosphides: A General Strategy for the Synthesis of Metal Phosphide Nanocrystals. *J. Am. Chem. Soc.* **2007**, *129* (7), 1896–1897. https://doi.org/10.1021/ja068502l.

(35) Knowles, K. E.; Hartstein, K. H.; Kilburn, T. B.; Marchioro, A.; Nelson, H. D.; Whitham, P. J.; Gamelin, D. R. Luminescent Colloidal Semiconductor Nanocrystals Containing Copper: Synthesis, Photophysics, and Applications. *Chem. Rev.* **2016**, *116* (18), 10820–10851. https://doi.org/10.1021/acs.chemrev.6b00048.

(36) Knowles, K. E.; Nelson, H. D.; Kilburn, T. B.; Gamelin, D. R. *Singlet–Triplet Splittings in the Luminescent Excited States of Colloidal Cu+:CdSe, Cu+:InP, and CuInS2 Nanocrystals: Charge-Transfer Configurations and Self-Trapped Excitons*. https://doi.org/10.1021/jacs.5b08547.

(37) Nelson, H. D.; Li, X.; Gamelin, D. R. Computational Studies of the Electronic Structures of Copper-Doped CdSe Nanocrystals: Oxidation States, Jahn–Teller Distortions, Vibronic Bandshapes, and Singlet–Triplet Splittings. *J. Phys. Chem. C* **2016**, *120* (10), 5714–5723. https://doi.org/10.1021/acs.jpcc.5b11319.

(38) Gary, D. C.; Flowers, S. E.; Kaminsky, W.; Petrone, A.; Li, X.; Cossairt, B. M. Single-Crystal and Electronic Structure of a 1.3 Nm Indium Phosphide Nanocluster. *J. Am. Chem. Soc.* **2016**, *138* (5), 1510–1513. https://doi.org/10.1021/jacs.5b13214.

(39) Bhuse, V. M.; Hankare, P. P.; Garadkar, K. M.; Khomane, A. S. A Simple, Convenient, Low Temperature Route to Grow Polycrystalline Copper Selenide Thin Films. *Materials Chemistry and Physics* **2003**, *80* (1), 82–88. https://doi.org/10.1016/S0254-0584(02)00306-1.

(40) Liu, Y.; Liu, M.; Swihart, M. T. Plasmonic Copper Sulfide-Based Materials: A Brief Introduction to Their Synthesis, Doping, Alloying, and Applications. *J. Phys. Chem. C* **2017**, *121* (25), 13435–13447. https://doi.org/10.1021/acs.jpcc.7b00894.

(41) White, S. L.; Banerjee, P.; Jain, P. K. Liquid-like Cationic Sub-Lattice in Copper Selenide Clusters. *Nat Commun* **2017**, *8* (1), 14514. https://doi.org/10.1038/ncomms14514.

(42) Liu, Z.; Zhong, Y.; Shafei, I.; Jeong, S.; Wang, L.; Nguyen, H. T.; Sun, C.-J.; Li, T.; Chen, J.; Chen, L.; Losovyj, Y.; Gao, X.; Ma, W.; Ye, X. Broadband Tunable Mid-Infrared Plasmon Resonances in Cadmium Oxide Nanocrystals Induced by Size-Dependent Nonstoichiometry. *Nano Lett.* **2020**, *20* (4), 2821–2828. https://doi.org/10.1021/acs.nanolett.0c00542.

(43) Schimpf, A. M.; Thakkar, N.; Gunthardt, C. E.; Masiello, D. J.; Gamelin, D. R. Charge-Tunable Quantum Plasmons in Colloidal Semiconductor Nanocrystals. *ACS Nano* **2014**, *8* (1), 1065–1072. https://doi.org/10.1021/nn406126u.

(44) Jharimune, S.; Sathe, A. A.; Rioux, R. M. Thermochemical Measurements of Cation Exchange in CdSe Nanocrystals Using Isothermal Titration Calorimetry. *Nano Lett.* **2018**, *18* (11), 6795–6803. https://doi.org/10.1021/acs.nanolett.8b02661.

(45) Hafiz, S. B.; Scimeca, M. R.; Zhao, P.; Paredes, I. J.; Sahu, A.; Ko, D.-K. Silver Selenide Colloidal Quantum Dots for Mid-Wavelength Infrared Photodetection. *ACS Appl. Nano Mater.* **2019**, *2* (3), 1631–1636. https://doi.org/10.1021/acsanm.9b00069.

(46) León-Velázquez, M. S.; Irizarry, R.; Castro-Rosario, M. E. Nucleation and Growth of Silver Sulfide Nanoparticles. *J. Phys. Chem. C* **2010**, *114* (13), 5839–5849. https://doi.org/10.1021/jp911238a.

(47) Akamatsu, K.; Takei, S.; Mizuhata, M.; Kajinami, A.; Deki, S.; Takeoka, S.; Fujii, M.; Hayashi, S.; Yamamoto, K. Preparation and Characterization of Polymer Thin Films Containing Silver and Silver Sulfide Nanoparticles. *Thin Solid Films* **2000**, *359* (1), 55–60. https://doi.org/10.1016/S0040-6090(99)00684-7.

(48) Mourdikoudis, S.; Liz-Marzán, L. M. Oleylamine in Nanoparticle Synthesis. *Chem. Mater.* **2013**, *25* (9), 1465–1476. https://doi.org/10.1021/cm4000476.

(49) *Materials Data on Cu3P by Materials Project*; mp-7463; Lawrence Berkeley National Lab. (LBNL), Berkeley, CA (United States). LBNL Materials Project, 2020. https://doi.org/10.17188/1288438.

(50) *Materials Data on PAu3 by Materials Project*; mp-1186369; Lawrence Berkeley National Lab. (LBNL), Berkeley, CA (United States). LBNL Materials Project, 2020. https://doi.org/10.17188/1695217.

(51) White, S. L.; Smith, J. G.; Behl, M.; Jain, P. K. Co-Operativity in a Nanocrystalline Solid-State Transition. *Nat Commun* **2013**, *4* (1), 2933. https://doi.org/10.1038/ncomms3933.

(52) Yao, Y.; Lynch, R.; Robinson, R. D. Mass Spectroscopy Study of the Intermediate Magic-Size Cluster Species during Cooperative Cation Exchange. *The Journal of Chemical Physics* **2023**, *159* (1), 014704. https://doi.org/10.1063/5.0151904.

(53) Taylor, M. G.; Kulik, H. J. Mapping the Origins of Surface- and Chemistry-Dependent Doping Trends in III–V Quantum Dots with Density Functional Theory. *Chem. Mater.* **2021**, *33* (17), 7113–7123. https://doi.org/10.1021/acs.chemmater.1c02556.

(54) Zhang, X.; Kim, D.; Guo, X.; Zhu, Y.; Lee, L. Y. S. Impacts of Boron Doping on the Atomic Structure, Stability, and Photocatalytic Activity of Cu3P Nanocrystals. *Applied Catalysis B: Environmental* **2021**, *298*, 120515. https://doi.org/10.1016/j.apcatb.2021.120515.

(55) Chowdari, B. V. R.; Mok, K. F.; Xie, J. M.; Gopalakrishnan, R. Spectroscopic and Electrical Studies of Silver Sulfophosphate Glasses. *Journal of Non-Crystalline Solids* **1993**, *160* (1), 73–81. https://doi.org/10.1016/0022-3093(93)90286-7.

(56) Kitagawa, H.; Kojima, N.; Nakajima, T. Studies of Mixed-Valence States in Three-Dimensional Halogen-Bridged Gold Compounds, Cs2AuIAuIIIX6, (X = Cl, Br or I). Part 2. X-Ray Photoelectron Spectroscopic Study. *J. Chem. Soc., Dalton Trans.* **1991**, No. 11, 3121–3125. https://doi.org/10.1039/DT9910003121.

(57) Wang, X.; Fei, Y.; Li, W.; Yi, L.; Feng, B.; Pan, Y.; Hu, W.; Li, C. M. Gold-Incorporated Cobalt Phosphide Nanoparticles on Nitrogen-Doped Carbon for Enhanced Hydrogen Evolution Electrocatalysis. *ACS Appl. Mater. Interfaces* **2020**, *12* (14), 16548–16556. https://doi.org/10.1021/acsami.0c02076.

(58) Tao, Y.; Yelon, A.; Sacher, E.; Lu, Z. H.; Graham, M. J. S-passivated InP (100)-(1×1) Surface Prepared by a Wet Chemical Process. *Appl. Phys. Lett.* **1992**, *60* (21), 2669–2671. https://doi.org/10.1063/1.106890.

(59) Freeland, B. H.; Habeeb, J. J.; Tuck, D. G. Coordination Compounds of Indium. Part XXXIII. X-Ray Photoelectron Spectroscopy of Neutral and Anionic Indium Halide Species. *Can. J. Chem.* **1977**, *55* (9), 1527–1532. https://doi.org/10.1139/v77-213.

(60) Mundy, M. E.; Eagle, F. W.; Hughes, K. E.; Gamelin, D. R.; Cossairt, B. M. Synthesis and Spectroscopy of Emissive, Surface-Modified, Copper-Doped Indium Phosphide Nanocrystals. *ACS Materials Lett.* **2020**, *2* (6), 576–581. https://doi.org/10.1021/acsmaterialslett.0c00112.

(61) Eagle, F. W.; Harvey, S.; Beck, R.; Li, X.; Gamelin, D. R.; Cossairt, B. M. Enhanced Charge Transfer from Coinage Metal Doped InP Quantum Dots. *ACS Nanosci. Au* **2023**. https://doi.org/10.1021/acsnanoscienceau.3c00029.

(62) Kwon, Y.; Oh, J.; Lee, E.; Lee, S. H.; Agnes, A.; Bang, G.; Kim, J.; Kim, D.; Kim, S. Evolution from Unimolecular to Colloidal-Quantum-Dot-like Character in Chlorine or Zinc Incorporated InP Magic Size Clusters. *Nat Commun* **2020**, *11* (1), 3127. https://doi.org/10.1038/s41467-020-16855-9.

(63) Okuda, Y.; Tsurumaki, E.; Oh, J.; Sung, J.; Kim, D.; Osuka, A. A Directly Fused Subporphyrin Dimer with a Wavelike Structure. *Angewandte Chemie International Edition* **2016**, *55* (32), 9212–9215. https://doi.org/10.1002/anie.201603759.

(64) Gary, D. C.; Petrone, A.; Li, X.; Cossairt, B. M. Investigating the Role of Amine in InP Nanocrystal Synthesis: Destabilizing Cluster Intermediates by Z-Type Ligand Displacement. *Chem. Commun.* **2016**, *53* (1), 161–164. https://doi.org/10.1039/C6CC07952K.

(65) Anderson, N. C.; Hendricks, M. P.; Choi, J. J.; Owen, J. S. Ligand Exchange and the Stoichiometry of Metal Chalcogenide Nanocrystals: Spectroscopic Observation of Facile Metal-Carboxylate Displacement and Binding. *J. Am. Chem. Soc.* **2013**, *135* (49), 18536–18548. https://doi.org/10.1021/ja4086758.

(66) Zhao, Q.; Kulik, H. J. Electronic Structure Origins of Surface-Dependent Growth in III–V Quantum Dots. *Chem. Mater.* **2018**, *30* (20), 7154–7165. https://doi.org/10.1021/acs.chemmater.8b03125.

(67) Shim, D.; Kang, J. Enhanced Reactivity of Magic-Sized Inorganic Clusters by Engineering the Surface Ligand Networks. *Chem. Mater.* **2023**, *35* (2), 700–708. https://doi.org/10.1021/acs.chemmater.2c03394.

(68) Zhang, F.; Chen, K.; Jiang, X.; Wang, Y.; Ge, Y.; Wu, L.; Xu, S.; Bao, Q.; Zhang, H. Nonlinear Optical Absorption and Ultrafast Carrier Dynamics of Copper Antimony Sulfide Semiconductor Nanocrystals. *J. Mater. Chem. C* **2018**, *6* (33), 8977–8983. https://doi.org/10.1039/C8TC01606B.

(69) Shi, G.; He, C.; Li, Y.; Zou, R.; Zhang, X.; Wang, Y.; Yang, K.; Song, Y.; Wang, C. H. Excited-State Nonlinearity Measurements of $ZnPcBr_4$/DMSO. *J. Opt. Soc. Am. B, JOSAB* **2009**, *26* (4), 754–761. https://doi.org/10.1364/JOSAB.26.000754.

(70) Kriegel, I.; Jiang, C.; Rodríguez-Fernández, J.; Schaller, R. D.; Talapin, D. V.; da Como, E.; Feldmann, J. Tuning the Excitonic and Plasmonic Properties of Copper Chalcogenide Nanocrystals. *J. Am. Chem. Soc.* **2012**, *134* (3), 1583–1590. https://doi.org/10.1021/ja207798q.

(71) Wang, Y.; Zhang, Y.; Wang, F.; Giblin, D. E.; Hoy, J.; Rohrs, H. W.; Loomis, R. A.; Buhro, W. E. The Magic-Size Nanocluster (CdSe)34 as a Low-Temperature Nucleant for Cadmium Selenide Nanocrystals; Room-Temperature Growth of Crystalline Quantum Platelets. *Chem. Mater.* **2014**, *26* (7), 2233–2243. https://doi.org/10.1021/cm404068e.

(72) Cumberland, S. L.; Hanif, K. M.; Javier, A.; Khitrov, G. A.; Strouse, G. F.; Woessner, S. M.; Yun, C. S. Inorganic Clusters as Single-Source Precursors for Preparation of CdSe, ZnSe, and CdSe/ZnS Nanomaterials. *Chem. Mater.* **2002**, *14* (4), 1576–1584. https://doi.org/10.1021/cm010709k.

(73) Li, L.; Zhang, J.; Zhang, M.; Rowell, N.; Zhang, C.; Wang, S.; Lu, J.; Fan, H.; Huang, W.; Chen, X.; Yu, K. Fragmentation of Magic-Size Cluster Precursor Compounds into Ultrasmall CdS Quantum Dots with Enhanced Particle Yield at Low Temperatures. *Angewandte Chemie* **2020**, *132* (29), 12111–12119. https://doi.org/10.1002/ange.202001608.

(74) *Materials Data on Ag3P by Materials Project*; mp-985295; Lawrence Berkeley National Lab. (LBNL), Berkeley, CA (United States). LBNL Materials Project, 2020. https://doi.org/10.17188/1272829.

TOC Graphic